


 Cite this: *RSC Adv.*, 2020, 10, 8352

# Structural study and large magnetocaloric entropy change at room temperature of $\text{La}_{1-x}\square_x\text{MnO}_3$ compounds

 C. Henchiri,<sup>a</sup> T. Mnasri,<sup>b</sup> A. Benali,<sup>ac</sup> R. Hamdi,<sup>ad</sup> E. Dhahri,<sup>a</sup> M. A. Valente<sup>c</sup> and B. F. O. Costa<sup>e</sup>

In this study, our central focus is to investigate the magnetocaloric characteristics of a  $\text{La}_{1-x}\square_x\text{MnO}_3$  ( $x = 0.1, 0.2$  and  $0.3$ ) series prepared by a sol–gel technique published in *Prog. Mater. Sci.*, **93**, 2018, 112–232. The crystallographic study revealed that our compounds crystallize in a rhombohedral structure with  $R\bar{3}c$ . Ferromagnetic (FM) and paramagnetic (PM) characters were detected from the variation in magnetization as a function of magnetic fields at different temperatures. The second order transition was verified from the Arrott plots ( $M^2$  vs.  $(\mu_0 H/M)$ ), where the slopes have a positive value. In order to verify the second order, we traced the variation of magnetization vs. temperature at different magnetic fields for  $x = 0.2$ . This revealed a ferromagnetic (FM)–paramagnetic (PM) transition when temperature increases. Relying on the indirect method while using the Maxwell formula, we determined the variation in the entropy ( $-\Delta S_M$ ) as a function of temperature for different magnetic fields for the three samples. We note that all the studied systems stand as good candidates for magnetic refrigeration with relative cooling power (RCP) values of around 131.4, 83.38 and 57.26  $\text{J kg}^{-1}$  with magnetic fields below 2 T, respectively. Subsequently, the magnetocaloric effect was investigated by a phenomenological model for  $x = 0.2$ . The extracted data confirm that this phenomenological model is appropriate for the prediction of magnetocaloric properties. The study also demonstrated that this  $\text{La}_{0.8}\square_{0.2}\text{MnO}_3$  system exhibits a universal behaviour.

 Received 12th December 2019  
 Accepted 10th February 2020

DOI: 10.1039/c9ra10469k

[rsc.li/rsc-advances](http://rsc.li/rsc-advances)

## 1. Introduction

Today, materials that have better properties have long drawn the interest and attention of researchers.<sup>1</sup> For this reason, there is a spate of interest in manganites because of their promising properties such as the colossal magnetoresistance (CMR), magnetocaloric effect of exchange (EME), Griffiths phase.<sup>2–8</sup> Perovskite-lanthanum manganites proved to be potential candidates for magnetic refrigeration at different temperature ranges.<sup>9–12</sup> Nanomaterials are expected to bring new features to the magnetocaloric effect (MCE) and magnetic properties compared to bulk materials.<sup>13,14</sup>

We note that there are numerous complex physical phenomena of manganites such as the charge ordering (CO). Swain *et al.* have shown that this phenomenon exists in nanomaterials. This is due to the planar defects and surface spin

disorder, *i.e.*, the deformation within a nanomaterial disturbs the AFM arrangement of the spins in the nucleus. Consequently, the state of the charge order is suppressed. However, for a bulk material the deformation is small as compared to a nanomaterial and that it has no impact on the AFM core and therefore, the appearance of the charge ordering (CO). More the suppression of the charge ordering (CO) in the materials can be due to the eruption of the spatial symmetry.<sup>15</sup> The charge ordering (CO) can be demonstrated from the electrical measurements. In the system  $\text{Pr}_{0.5}\text{Ca}_{0.5}\text{MnO}_3$ ,<sup>16</sup> the suppression of CO is explained by the melting of long-range charge ordering behavior due to surface spin disorder and induced lattice strain effects in PCMO manganite system.

Electric field controlled magnetism is an exciting area of condensed matter physics. It allows the exploration of device applications with ultra-low energy consumption compared to the conventional current-controlled or magnetic field-controlled devices. Numerous studies were performed by Swain *et al.* to demonstrate the electric field-controlled magnetoresistance (MR) in a three layer structure composed of  $\text{La}_{0.67}\text{Sr}_{0.33}\text{MnO}_3$  (LSMO) (40 nm)/ $\text{SrTiO}_3$  (10 nm)/LSMO (10 nm) grown *via* the pulsed laser deposition technique on a 500  $\mu\text{m}$  thick  $\text{BaTiO}_3$  (001) monocrystalline substrate (BTO). The jumps observed in the temperature-dependent magnetization

<sup>a</sup>Laboratoire de Physique Appliquée, Faculté des Sciences de Sfax, Université de Sfax, B. P. 802, Sfax 3018, Tunisia

<sup>b</sup>Research Unit UPIM, Faculty of Science, University of Gafsa, 2112, Tunisia

<sup>c</sup>3N, Physics Department, University of Aveiro, 3810-193 Aveiro, Portugal

<sup>d</sup>College of Health and Life Sciences, Hamad Bin Khalifa University, Doha, Qatar

<sup>e</sup>CFisUC, Physics Department, University of Coimbra, RuaLarga, 3004-516 Coimbra, Portugal


curve around the structural phase transitions of BTO ensure the magnetoelectric coupling mediated by the stress between the LSMO and BTO layers. A significant change in the MR of this structure in the applied electric fields shows no dependence on polarity. Results are linked to magnetoelectric coupling mediated by network constraint in ferromagnetic/ferroelectric LSMO BTO heterostructures.<sup>17</sup>

Today, a new technology called magnetic cooling offers several advantages, including higher cooling efficiency, lower power consumption, lower noise level, much compactness, and higher safety for the environment. This new technology rests on a phenomenon called “magnetocaloric effect” (MCE). Recent discoveries in materials science disclosed that colossal ECM values can be observed in many materials (manganites, ferrites, amorphous alloys, intermetallic compounds, *etc.*).<sup>18</sup> The magnetocaloric effect (MCE) is a basic character of magnetic materials. It is the response of the material to the application or suppression of magnetic fields. Relying upon the isothermal magnetic data, the magnetic entropy change ( $\Delta S_M$ ) can be assessed through the use of the standard Maxwell relation:<sup>19</sup>

$$\Delta S_M(T, \mu_0 H) = S_M(T, \mu_0 H) - S_M(T, 0) = \int_0^{\mu_0 H} \left( \frac{\partial S}{\partial \mu_0 H} \right)_T \mu_0 H \quad (1)$$

According to Maxwell's relation, we get

$$\left( \frac{\partial M}{\partial T} \right)_{\mu_0 H} = \left( \frac{\partial S}{\partial \mu_0 H} \right)_{\mu_0 H} \quad (2)$$

The extremums of the  $-\Delta S_M$  of our compounds are reported in the vicinity of  $T_C$ , where  $\left( \frac{\partial M}{\partial T} \right)_{\mu_0 H}$  is the experimental value obtained from the  $M(T)$  curve for multiple magnetic fields ( $\mu_0 H$ ).

Magnetic entropy change is provided by the following expression:

$$\Delta S_M \left( \frac{T_1 + T_2}{2} \right) = \left( \frac{1}{(T_2 - T_1)} \right) \left( \int_0^{\mu_0 H} M(T_2, \mu_0 H) \right) \mu_0 dH - \left( \int_0^{\mu_0 H} M(T_1, \mu_0 H) \right) \mu_0 dH \quad (3)$$

The entropy is connected to the relative cooling power (RCP) by the relation:<sup>20</sup>

$$\text{RCP} = |\Delta S_M^{\text{max}}| \times \delta T_{\text{FWHM}} \quad (4)$$

where  $\delta T_{\text{FWHM}}$  is the full width at half maximum of the magnetic entropy change curve. A good system for applications in the field of magnetic cooling must be characterized by a large heat capacity defined by:

$$\Delta C_P(T, \mu_0 H) = C_P(T, \mu_0 H) - C_P(T, 0) = T \frac{\partial(\Delta S_M(T, \mu_0 H))}{\partial T} \quad (5)$$

Features of manganites continuously have drawn the attention of multiple researchers specialized in condensed matter physics.<sup>21–26</sup> These compounds are known for their close relations between orbital, charge, spin, and lattice degrees of freedom, which results in a diversity of their phase states and physical properties.<sup>27–30</sup> Among the wide variety of factors specifying the properties of manganites, the most significant ones are the stoichiometry (the types of ions and their ratio) and crystal structure parameters (the mean  $\langle \text{Mn-O} \rangle$  bond length and the mean  $\langle \text{Mn-O-Mn} \rangle$  bond angle).

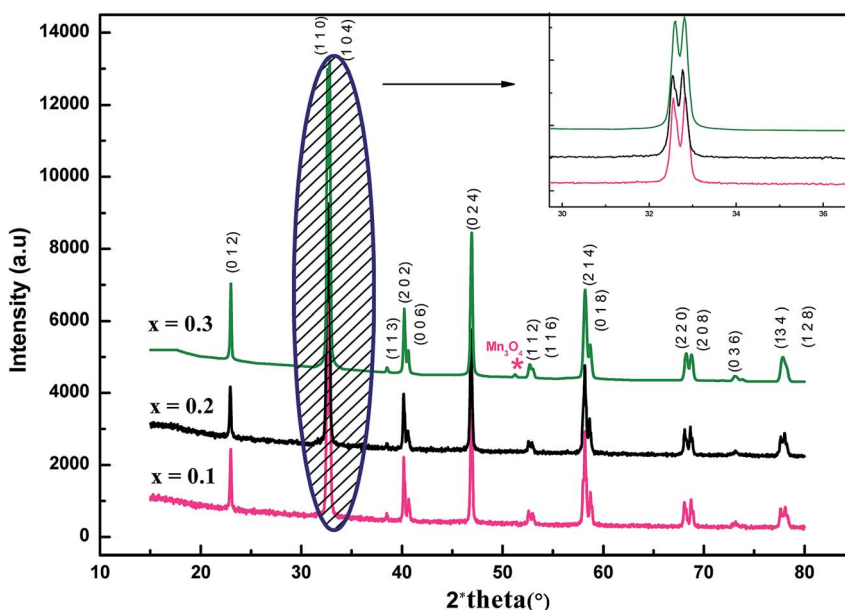


Fig. 1 XRD patterns of the  $\text{La}_{1-x}\square_x\text{MnO}_3$  ( $x = 0.1, 0.2$  and  $0.3$ ) compounds at room temperature.



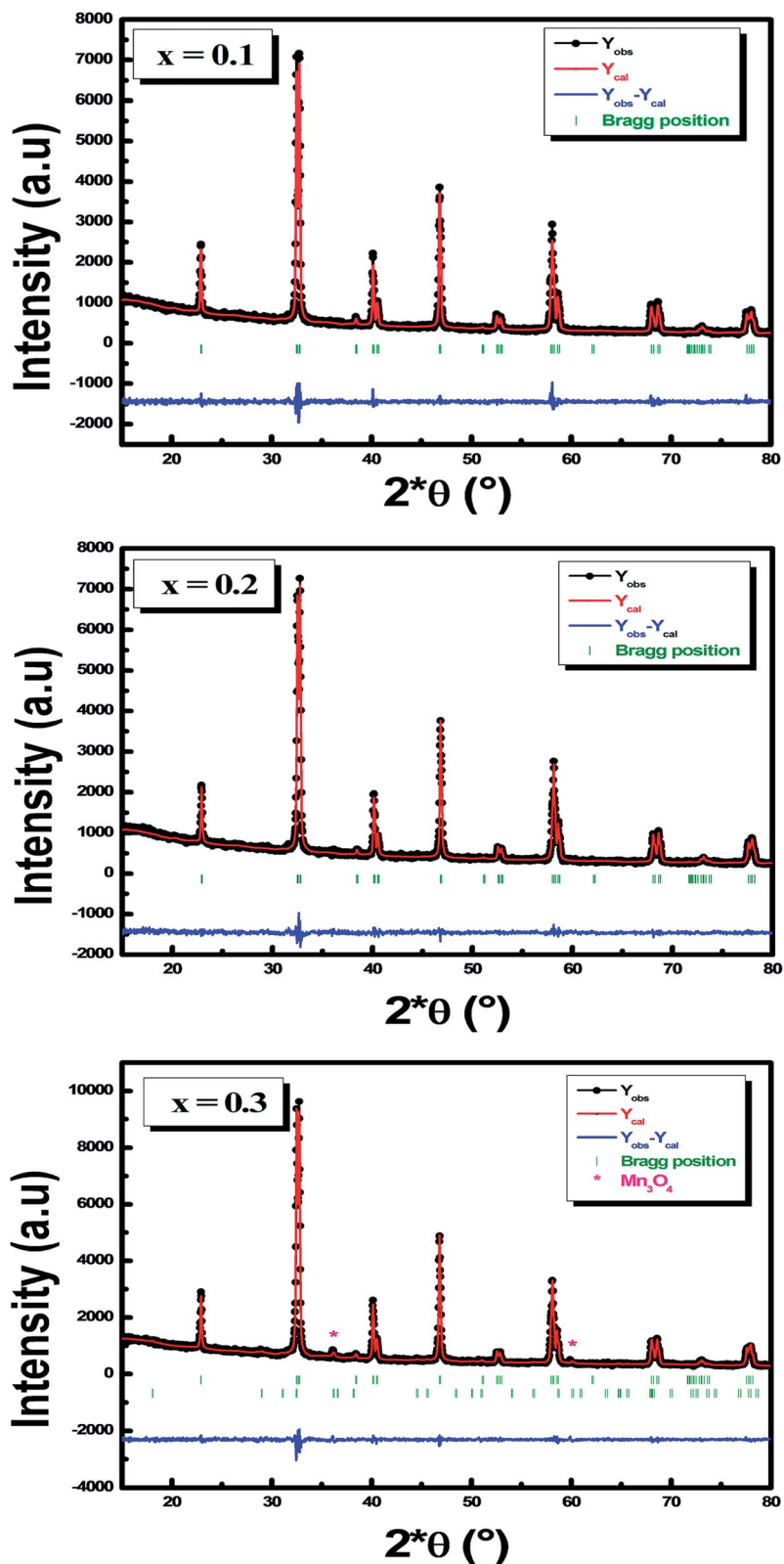


Fig. 2 Rietveld refinement of the X-ray patterns of  $\text{La}_{1-x}\square_x\text{MnO}_3$  ( $x = 0.1, 0.2$  and  $0.3$ ). Experimental data presented in black, calculated data presented in red, difference between them presented in blue, Bragg position presented in green.





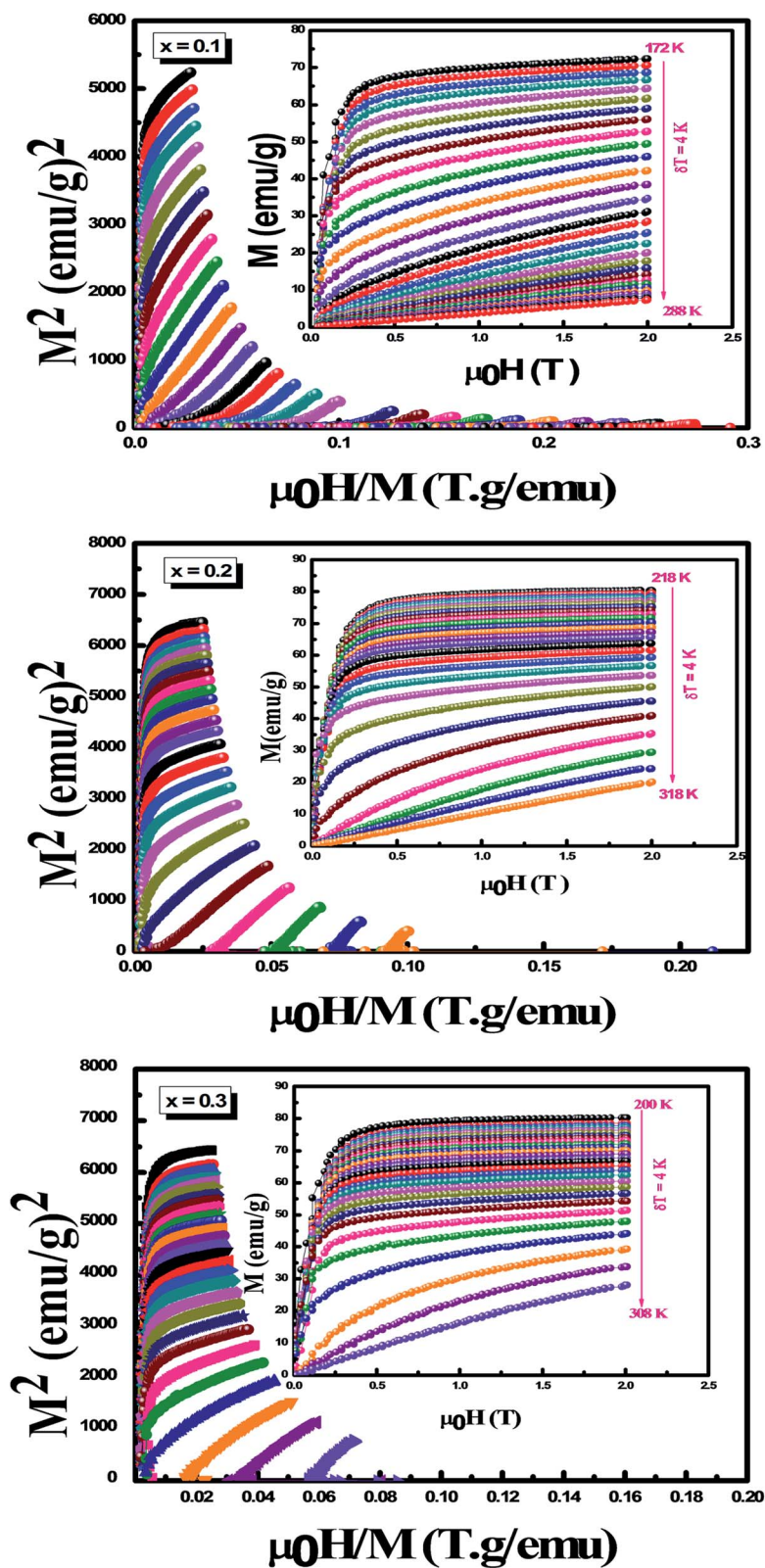


Fig. 4 Isothermal magnetization plots  $M$  versus  $H$  of the  $\text{La}_{1-x}\square_x\text{MnO}_3$  ( $x = 0.1, 0.2$  and  $0.3$ ) series, and the inset is the Standard Arrot.



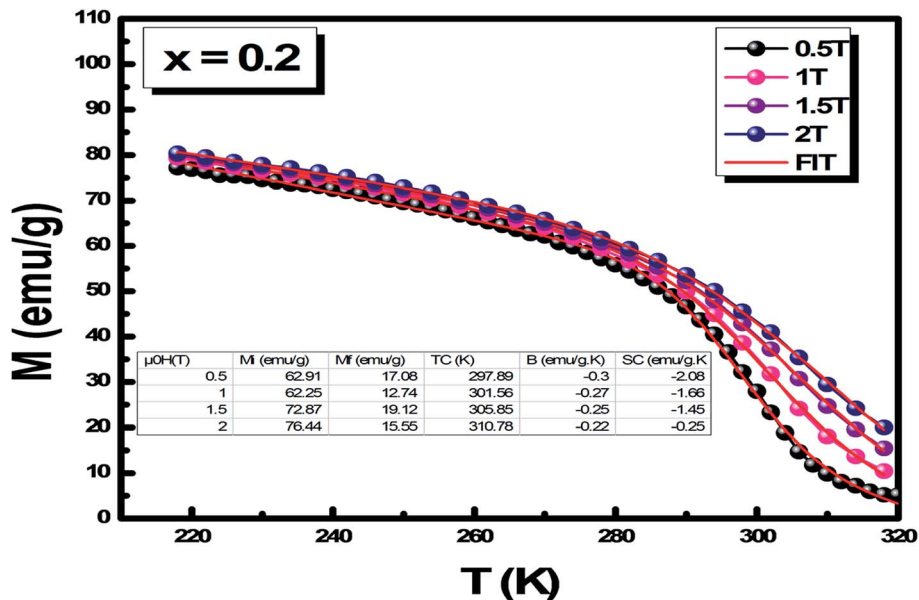


Fig. 5 Magnetization versus temperature for  $\text{La}_{0.8}\square_{0.2}\text{MnO}_3$ . The symbols are the experimental data and the solid lines are the modeled results.

It is conventionally known that the magnetic and electronic properties of substituted manganites are specified by the  $e_g$  electron bandwidth  $W = \cos(1/2[\pi - \langle \text{Mn-O-Mn} \rangle]) / \langle \text{Mn-O} \rangle^{3.5}$ .<sup>31</sup> Compounds with a greater bandwidth  $W$  display more pronounced ferromagnetic and metallic properties (*i.e.*, higher

Curie point ( $T_C$ ), higher metal insulator transition temperature and lower resistivity ( $\rho$ )<sup>32-34</sup>).

This study centers around the magnetocaloric effect and Hamed model for the three compounds,  $x = 0.1, 0.2$  and  $0.3$ .

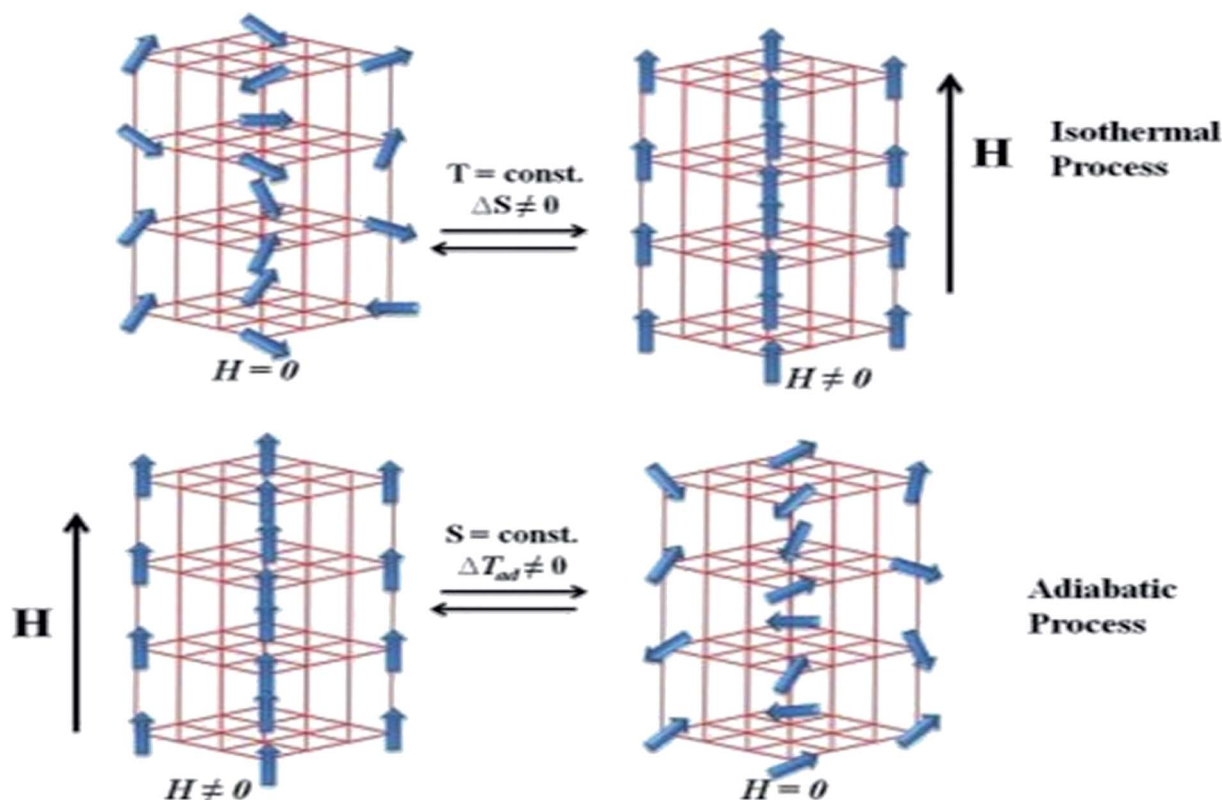


Fig. 6 Schematic representation for the magnetic refrigeration cycle.



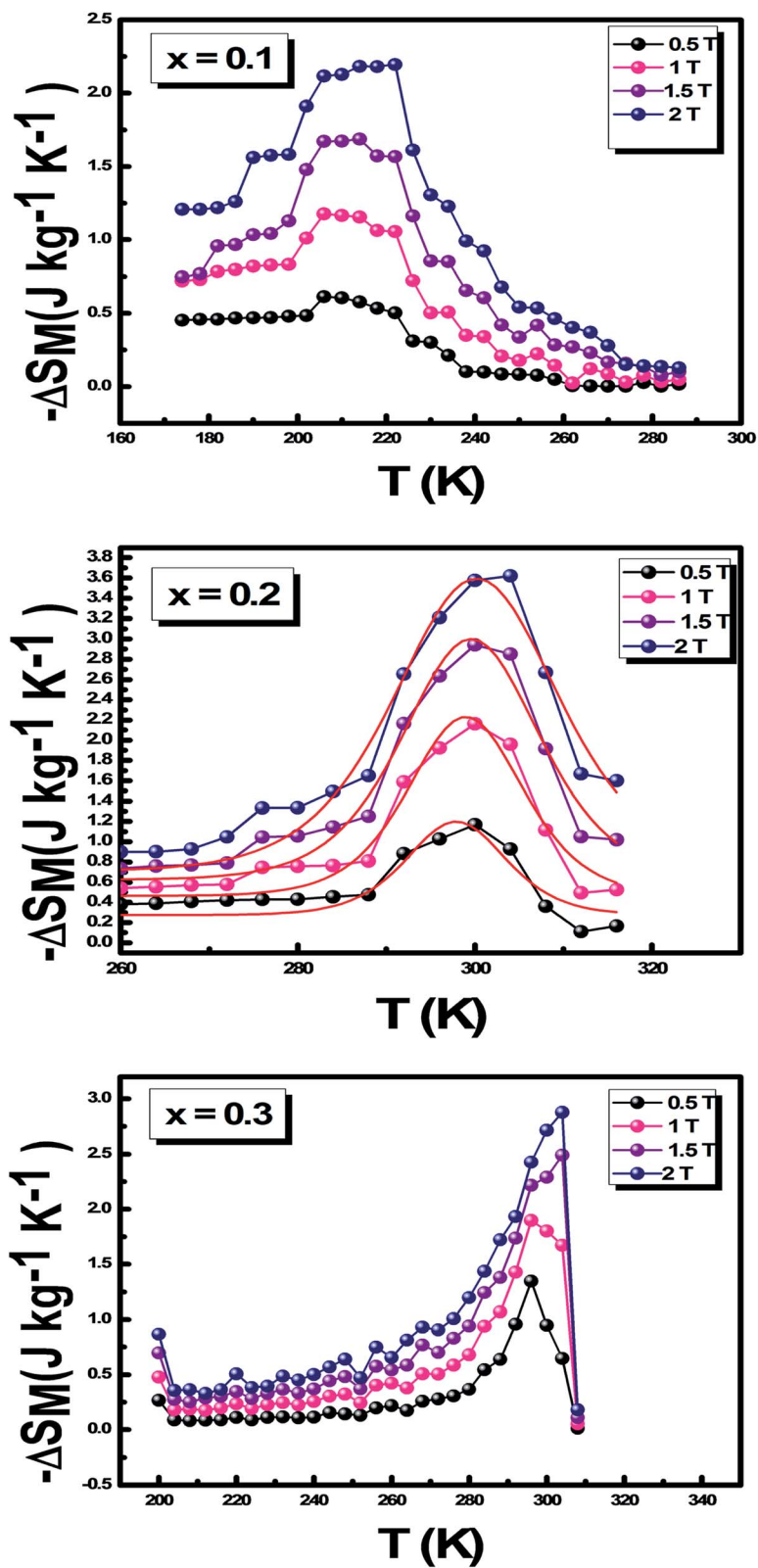


Fig. 7 Thermal variation of the magnetic entropy ( $-\Delta S_M$ ) of  $\text{La}_{1-x}\square_x\text{MnO}_3$  ( $x = 0.1, 0.2$  and  $0.3$ ) systems under different magnetic fields between 0.5 T and 2 T and modeled for  $x = 0.2$ .



## 2. Preparation method

The sol-gel technique is the preparation method of  $\text{La}_{1-x}\square_x\text{MnO}_3$  ( $x = 0.1, 0.2$  and  $0.3$ ) from the precursors lanthanum nitrate ( $\text{La}(\text{NO}_3)_3 \cdot 6\text{H}_2\text{O}$ ) and manganese nitrate ( $\text{Mn}(\text{NO}_3)_2 \cdot 4\text{H}_2\text{O}$ ) up to purity 99%. The method of preparation has been well described in ref. 35.

## 3. Results and discussion

In the first step, we performed XRD analysis to verify the crystal structure of the studied samples. Powder XRD patterns of  $\text{La}_{1-x}\square_x\text{MnO}_3$  ( $x = 0.1, 0.2$  and  $0.3$ ) compounds collected at room temperature are plotted in Fig. 1. We note that our samples are of a single phase with a very small amount of  $\text{Mn}_3\text{O}_4$  for  $x = 0.3$ , as found in recent studies.<sup>35</sup> XRD data were analyzed using Rietveld refinement.<sup>36</sup> Fig. 2 illustrates the Rietveld refinement of the XRD profiles for  $\text{La}_{1-x}\square_x\text{MnO}_3$  ( $x = 0.1, 0.2$  and  $0.3$ ) samples, with a good agreement between the observed and the calculated profiles, this is due to the excellent goodness of  $\chi^2$ . The analyzed data showed that our samples crystallize in the rhombohedral system with  $R\bar{3}c$ . The SEM micrographs of Fig. 3 show a non-homogenous microstructure and non-uniform grain size distribution. In order to check the existence of all elements in the compound, EDX was performed. Fig. 3 shows that the energy dispersive analysis of X-ray (EDX) spectra reveals the presence of La, Mn and O elements in  $\text{La}_{1-x}\square_x\text{MnO}_3$  compounds, confirming that there is no loss of any integrated element. In order to examine the distribution of detected elements, the EDX mapping of La (slate blue), Mn (green) and O (red) is checked and presents non uniform dispersion. All samples reveal the presence of the characteristic peaks of La and Mn and O elements. The inset curves in Fig. 4

display the magnetic isotherms of  $x = 0.1, 0.2$  and  $0.3$  samples measured with a magnetic field change from 0 to 2 T in the temperature interval of 4 K. Here, the maximum magnetization is recorded for  $x = 0.2$  and  $0.3$  samples, suggesting that adiabatic magnetization and demagnetization result in the maximum order and disorder in these samples. The Arrott plots (Fig. 4) exhibit the variation of  $M^2$  vs.  $\mu_0 H/M$  for the three compounds ( $x = 0.1, 0.2$  and  $0.3$ ) to determine the nature of transition (first order: negative slope and second order: positive slope). We notice that these curves have a positive slope, which indicates that the transition from the FM to the PM state at the Curie temperature ( $T_C$ ) is a second order magnetic phase transition, according to the criteria reported by Banerjee.<sup>37</sup>

In order to apply the phenomenological model,<sup>38,39</sup> Fig. 3 depicts the variation in the magnetization  $M$  as a function of temperature at various magnetic applied fields for  $x = 0.2$ . Experimental data (symbols) were modified by the eqn (1)<sup>40</sup> (solid line). We find that this equation well portrays the pace of magnetization, which proves the validity of this model in our case. Model parameters are presented in table in the inset Fig. 5. Furthermore, the curves  $M(H, T)$  at  $\mu_0 H$  unveil the presence of a second order paramagnetic-ferromagnetic transition, where the magnetization varies from continuous way deduced from the increase in  $T_C$  with the magnetic field.

Fig. 6 portrays the schematic representation of the magnetic refrigeration cycle whose value of the change in entropy of a ferromagnetic material depends on both  $\mu_0 H$  and  $T$ . Fig. 7 illustrates the variation in the magnetic entropy change ( $-\Delta S_M$ ) as a function of  $T$  for different  $\mu_0 H$  using eqn (3) for the three samples  $x = 0.1, 0.2$  and  $0.3$ . It increases by augmenting the value of  $\mu_0 H$  and reaches a maximum around  $T_C$ . For  $x = 0.2$  and using eqn (5),<sup>40</sup> we plot the theoretical entropy as a function of magnetic field for  $x = 0.2$ . We can assert that the maximum

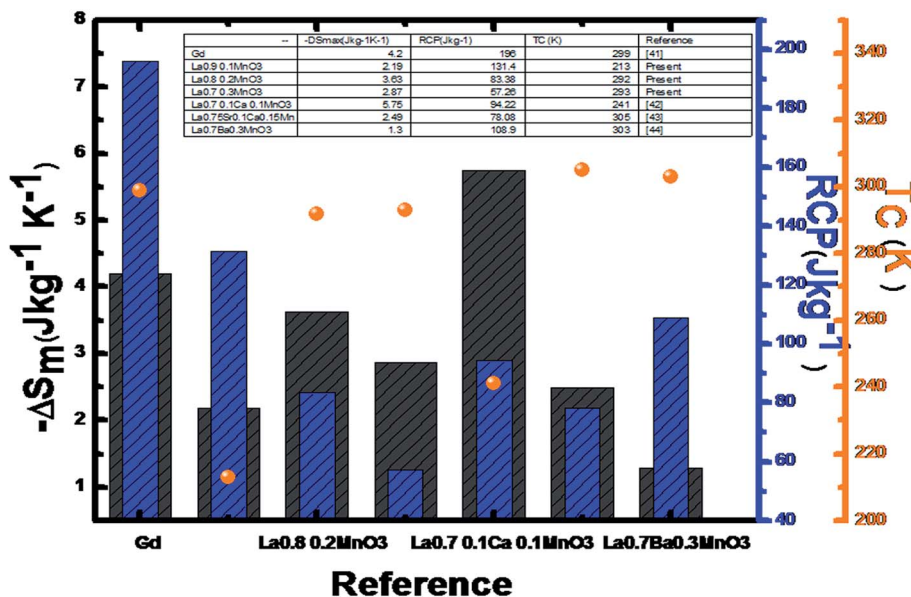


Fig. 8 Comparative histogram representation of the values of  $(-\Delta S_M)$ , RCP and Curie temperature ( $T_C$ ) at 2 T for  $\text{La}_{1-x}\square_x\text{MnO}_3$  ( $x = 0.1, 0.2$  and  $0.3$ ) with the family of La-manganite materials and the standard gadolinium (Gd) sample. The dotted orange line shows the room temperature. The inset shows the table with corresponding materials with their respective references.



magnetic entropy is obtained around  $T_C$ . Zener model was appropriate to justify the change to perovskite large magnetic entropy. This model discloses an indirect interaction between  $Mn^{3+}$  and  $Mn^{4+}$  related to the change in their ratio.<sup>41</sup> Guo *et al.*<sup>42</sup> assumed that the large magnetic entropy change in perovskite manganites could refer to the spin-lattice coupling in the magnetic ordering process, which plays an intrinsic role in additional magnetic changes.<sup>43,44</sup>

The experimental values of  $(-\Delta S_M)$ , RCP and  $T_C$  for our compound are compared to other references at 2 T, which are listed in the inset table in Fig. 8. We observe that  $-\Delta S_M$

increases and RCP decreases. This is explained by the effect of spin coupling, which became less important when the applied magnetic field increased. We can detect that the proposed compounds exhibit important values. The maximum values of  $\Delta S_M$  and RCP obtained at 2 T were compared to gadolinium  $Gd^{45}$  as well as several other materials reported in literature.<sup>46-48</sup> The results are in favor of promising magnetic refrigerants in terms of application. The good value of RCP equal to  $131.4 J kg^{-1}$  for  $x = 0.1$  is due to the strong magneto-structural coupling.

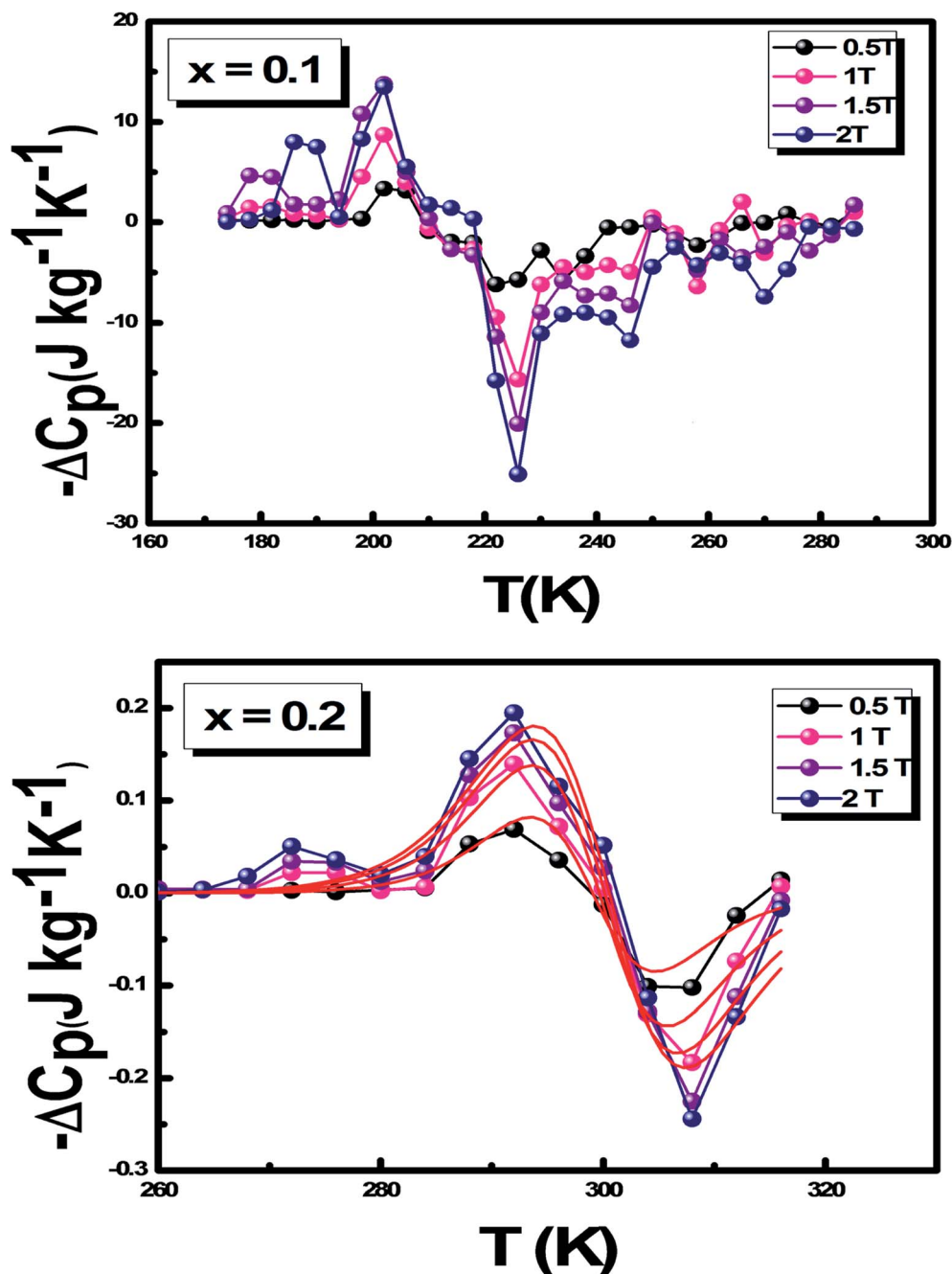


Fig. 9 Variation in the specific heat as a function of temperature at different magnetic fields of  $La_{1-x}\square_xMnO_3$  ( $x = 0.1$  and  $0.2$ ) and modeled for  $x = 0.2$ .



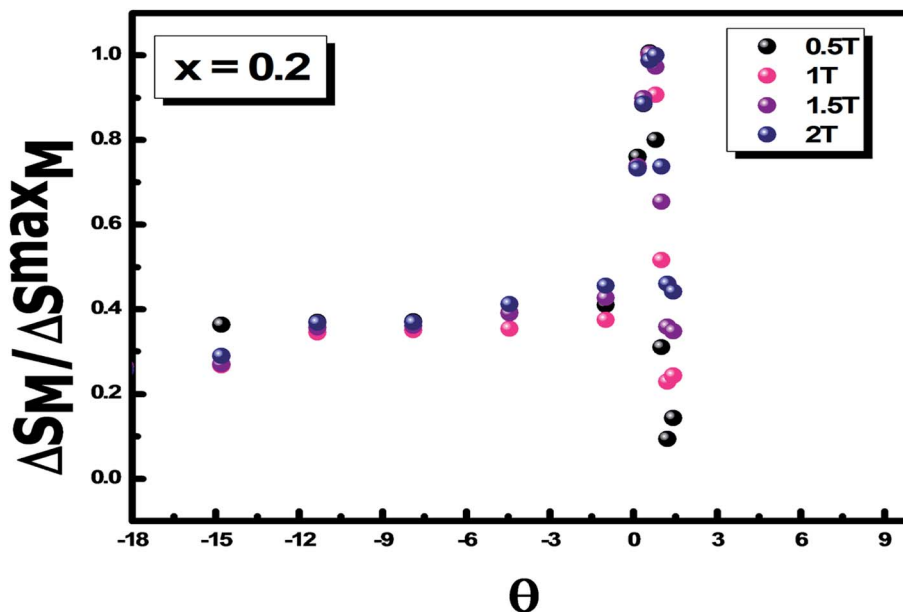


Fig. 10 The universal curve for  $x = 0.2$ .

Using eqn (5), we plot the experimental  $(-\Delta C_p)$  as a function of temperature for  $x = 0.1$  and  $0.2$  in Fig. 9. Using eqn (6),<sup>40</sup> we plot the theoretical variation of  $(-\Delta C_p)$  for  $x = 0.2$  as an example. This figure demonstrates that the intersection of these curves is around  $T_C$ . It is clear that  $(-\Delta C_p)$  is positive when  $T_C > T$  and negative when  $T_C < T$ .

A universal behavior of  $\Delta S_M$  and its dependence on the field in materials with a second order transition have recently been proposed by Franco *et al.*,<sup>49,50</sup> who set forward a universal behavior of  $-\Delta S_M$ . The phenomenological universal curve consists of the collapse of the entropy variation curves after a scaling process, regardless of the applied magnetic field. Therefore, the main hypothesis is based on the fact that if a universal curve exists, then the equivalent points of  $\Delta S_M(T)$  curves measured for different applied magnetic fields should collapse on the same universal curve. It is also demonstrated that these curves are unique for each class of universality.<sup>50</sup> MCE data from different materials of the same universality class should overlap on the same curve regardless of the applied magnetic field.

This phenomenological universal curve can be established by normalizing all  $\Delta S_M(T)$  curves by their respective maximum value,  $\Delta S_M^{\max}$ , as a function of  $\Delta S'_M = \Delta S_M/2$ , and the temperature axis are rescaled by a new parameter  $\theta = \pm 1$ , identified by the expression:

$$\theta = \begin{cases} -\frac{T - T_C}{T_{r1} - T_C}, & T \leq T_C \\ \frac{T - T_C}{T_{r2} - T_C}, & T > T_C \end{cases} \quad (6)$$

$T_{r1}$  and  $T_{r2}$  are the temperature values of the two reference points on each curve.

Fig. 10 illustrates the universal curve for  $x = 0.2$  (as an example). We can clearly infer that all the curves collapse on

a single universal curve regardless of the magnetic field, which proves the validity of the technique and suggests that the transition is of a second order.

## 4. Conclusion

In this study, we investigated the magnetocaloric effects of  $\text{La}_{1-x}\text{MnO}_3$  ( $x = 0.1, 0.2$  and  $0.3$ ) prepared *via* a sol-gel technique. We demonstrated that our samples displayed a second order transition, as implied from the Arrot plot. In order to verify the second order, we traced the variation of  $M$  vs.  $T$  at different magnetic fields for  $x = 0.2$ . This exhibited an FM-PM transition when the temperature increased. Based upon the Maxwell formula, we determined the variation in the entropy  $(-\Delta S_M)$  as a function of temperature for different magnetic fields for the three samples. It is noteworthy to mention that all studied systems stand as good candidates for magnetic refrigeration at about 131.4, 83.38 and 57.26  $\text{J kg}^{-1}$  with magnetic fields under to 2 T, respectively. The study also proved that this  $\text{La}_{0.8}\text{MnO}_3$  system presents a universal behaviour. After exploring the magnetocaloric effect by a phenomenological model for  $x = 0.2$ , the extracted data confirm that this phenomenological model is convenient for the prediction of magnetocaloric properties.

Being a promising compound, in future studies, we aspire to further explore its additional interesting features so as to be invested in technological as well as industrial fields.

## Conflicts of interest

There are no conflicts to declare.



## Acknowledgements

The authors acknowledge the financial support of the research project by the Tunisian Ministry of Higher Education and Scientific Research and the FCT-Portugal within the framework of Tunisian-Portuguese cooperation in the field of scientific research and technology.

## References

- 1 P. T. Phong, N. V. Dang, L. V. Bau, N. M. An and In-Ja Lee, Landau mean-field analysis and estimation of the spontaneous magnetization from magnetic entropy change in  $\text{La}_{0.7}\text{Sr}_{0.3}\text{MnO}_3$  and  $\text{La}_{0.7}\text{Sr}_{0.3}\text{Mn}_{0.95}\text{Ti}_{0.05}\text{O}_3$ , *J. Alloys Compd.*, 2017, **698**, 451–459.
- 2 K. Y. Wang, C. Sangregorio, J. Wiggins, J. Wiemann and J. Tang, Colossal magnetoresistance and magnetic phase transitions in bulk  $\text{Nd}_{0.7}\text{Ba}_{0.3}\text{MnO}_3$ , *J. Appl. Phys.*, 2000, **87**, 5819–5821.
- 3 F. B. Jemaa, S. H. Mahmood, M. Ellouze, E. K. Hlil and F. Halouani, Structural, magnetic, magnetocaloric, and critical behavior of selected Ti-doped manganites, *Ceram. Int.*, 2015, **41**, 8191–8202.
- 4 P. T. Phong, L. V. Bau, L. C. Hoan, D. H. Manh, N. X. Phuc and In-Ja Lee, Effect of B-site Ti doping on the magnetic, low-field magnetocaloric and electrical transport properties of  $\text{La}_{0.7}\text{Sr}_{0.3}\text{Mn}_{1-x}\text{Ti}_x\text{O}_3$  perovskites, *J. Alloys Compd.*, 2016, **656**, 920–928.
- 5 S. E. L. Kossi, S. Ghodhbane, S. Mnefui, J. Dhahri and E. K. Hlil, The impact of disorder on magnetocaloric properties in Ti-doped manganites of  $\text{La}_{0.7}\text{Sr}_{0.25}\text{Na}_{0.05}\text{Mn}_{(1-x)}\text{Ti}_x\text{O}_3$  ( $0 \leq x \leq 0.2$ ), *J. Magn. Magn. Mater.*, 2015, **395**, 134–142.
- 6 S. Liu, Magnetocaloric effect of electron-doped manganites  $\text{LaMn}_{1-x}\text{Ti}_x\text{O}_3$  ( $0.05 \leq x \leq 0.2$ ), *Phys. B*, 2015, **456**, 227–231.
- 7 A. Sendil Kumar and S. Srinath, Exchange bias effect in Ti doped nanocrystalline  $\text{SrFeO}_{3-\delta}$ , *AIP Adv.*, 2014, **4**, 087144–087148.
- 8 V. Dayal, V. P. Kumar, R. L. Hadimani and D. C. Jiles, Evolution of Griffith's phase in  $\text{La}_{0.4}\text{Bi}_{0.6}\text{Mn}_{1-x}\text{Ti}_x\text{O}_3$  perovskite oxide, *J. Appl. Phys.*, 2014, **115**, 17E111.
- 9 H. Y. Hwang, S. W. Cheong, N. P. Ong and B. Batlogg, Spin-Polarized Intergrain Tunneling in  $\text{La}_{2/3}\text{Sr}_{1/3}\text{MnO}_3$ , *Phys. Rev. Lett.*, 1996, **77**, 2041–2044.
- 10 C. N. R. Rao, R. Mahesh, A. K. Raychaudhuri and R. Mahendiran, Giant magnetoresistance, charge ordering and other novel properties of perovskite manganates, *J. Phys. Chem. Solids*, 1998, **59**, 487–501.
- 11 B. C. Tofield and W. R. Scott, Oxidative nonstoichiometry in perovskites, an experimental survey; the defect structure of an oxidized lanthanum manganite by powder neutron diffraction, *J. Solid State Chem.*, 1974, **10**, 183–194.
- 12 N. Zhang, W. Ding, T. Tanx, W. Zhong and Y. Du, Simultaneous observation of tunnel-type GMR and intrinsic CMR in nanometer perovskite, *Sci. China, Ser. A: Math., Phys., Astron.*, 1998, **41**, 967–973.
- 13 L. J. S. R. D. Shull and L. H. Bennett, in *Proceedings of the 6th International Cryocoolers Conference*, ed. G. G. a. M. Knox, Annapolis, 1991, p. 231.
- 14 T. A. Yamamoto, M. Tanaka, Y. Misaka, T. Nakagawa, T. Nakayama, K. Niihara and T. Numazawa, Dependence of the magnetocaloric effect in superparamagnetic nanocomposites on the distribution of magnetic moment size, *Scr. Mater.*, 2002, **46**, 89–94.
- 15 A. Swain and V. Gorige, Irreversible Meta-Magnetic Transition in Charge Ordered  $\text{Nd}_{0.5}\text{Ca}_{0.5}\text{MnO}_3$  Manganite, *Phys. Status Solidi B*, 2019, 1800707.
- 16 A. Swain, P. S. Anil Kumar and V. Gorige, Electrical conduction mechanism for the investigation of charge ordering in  $\text{Pr}_{0.5}\text{Ca}_{0.5}\text{MnO}_3$  manganite system, *J. Magn. Magn. Mater.*, 2019, **485**, 358–368.
- 17 A. Swain, K. Komatsu, M. Itoh, T. Taniyama and V. Gorige, Strain-mediated magnetic response in  $\text{La}_{0.67}\text{Sr}_{0.33}\text{MnO}_3/\text{SrTiO}_3/\text{La}_{0.67}\text{Sr}_{0.33}\text{MnO}_3/\text{BaTiO}_3$  structure, *AIP Adv.*, 2018, **8**, 055808.
- 18 V. Franco, J. S. Blázquez, J. J. Ipus, J. Y. Law, L. M. Moreno-Ramírez and A. Conde, Magnetocaloric effect: from materials research to refrigeration devices, *Prog. Mater. Sci.*, 2018, **93**, 112–232, DOI: 10.1016/j.pmatsci.2017.10.005.
- 19 K. Vitalij, V. K. Pecharsky and K. A. Gschneidner Jr, Magnetocaloric effect and magnetic refrigeration, *J. Magn. Magn. Mater.*, 1999, **200**, 44–56.
- 20 K. A. Gschneidner Jr, V. K. Pecharsky and A. O. Tsokol, Recent developments in magnetocaloric materials, *Rep. Prog. Phys.*, 2005, **68**, 1479–1539.
- 21 S. V. Trukhanov, I. O. Troyanchuk, M. Hervieu, H. Szymczak and K. Bärner, *Phys. Rev. B: Condens. Matter*, 2002, **66**, 184424.
- 22 S. M. Dunaevskii, *Fiz. Tverd. Tela*, 2004, **46**(2), 193.
- 23 J. B. Goodenough, *Rep. Prog. Phys.*, 2004, **67**, 1915.
- 24 E. Dagotto, *New J. Phys.*, 2005, **7**, 67.
- 25 K. Dörr, *J. Phys. D: Appl. Phys.*, 2006, **39**, R125.
- 26 S. V. Trukhanov, L. S. Lobanovskii, A. V. Trukhanov, S. G. Zemskova and A. I. Beskrovniy, *Phys. Status Solidi C*, 2009, **6**, 1001.
- 27 J. M. D. Coey, M. Viret and S. von Molnar, *Adv. Phys.*, 1999, **48**, 167.
- 28 E. L. Nagaev, *Phys. Rep.*, 2001, **346**, 387.
- 29 S. V. Trukhanov, *Zh. Eksp. Teor. Fiz.*, 2005, **128**(3), 597; *J. Exp. Theor. Phys.*, 2005, **101**(3), 513.
- 30 S. V. Trukhanov, D. P. Kozlenko and A. V. Trukhanov, *J. Magn. Magn. Mater.*, 2008, **320**, e88.
- 31 M. Medarde, J. Mesot, P. Lacorre, S. Rosenkranz, P. Fischer and K. Gobrecht, *Phys. Rev. B: Condens. Matter*, 1995, **52**(3), 9248.
- 32 Y. Moritomo, A. Asamitsu and Y. Tokura, *Phys. Rev. B: Condens. Matter*, 1995, **51**, 16491.
- 33 Y. Moritomo, A. Asamitsu and Y. Tokura, *Phys. Rev. B: Condens. Matter*, 1997, **56**, 12190.
- 34 H. Y. Hwang, T. T. M. Palstra, S. W. Cheong and B. Batlogg, *Phys. Rev. B: Condens. Matter*, 1995, **52**, 15046.
- 35 C. Henchiri, R. Hamdi, T. Mnasri, M. AValente, P. R. Prezias and E. Dhahri, *Structural and magnetic properties of*



- $La_{1-x}Ca_xMnO_3$  ( $x = 0.1; 0.2$  and  $0.3$ ) manganites, 2019, DOI: 10.1007/s00339-019-2980-3.
- 36 D. B. Wiles and R. A. Young, *J. Appl. Crystallogr.*, 1981, **14**, 149–151.
- 37 S. K. Banerjee, On a generalized approach to first and second order magnetic transition, *Phys. Lett.*, 1964, **12**, 16–17.
- 38 M. A. Hamed, *Phase Transitions*, 2012, **85**, 106.
- 39 M. A. Hamed, *Mater. Lett.*, 2012, **82**, 181.
- 40 H. Gharsallah, M. Jeddi, M. Bejar, E. Dhahri and E. K. Hlil, Prediction of magnetocaloric effect using a phenomenological model in  $(x) La_{0.6}Ca_{0.4}MnO_3/(1 - x) La_{0.6}Sr_{0.4}MnO_3$  composites, *Appl. Phys.*, 2019, **125**, 541.
- 41 C. Zener, Interaction between the d shells in the transition metals, *Phys. Rev.*, 1951, **81**, 440.
- 42 Z. B. Guo, Y. M. Du, J. S. Zhu, H. Huang, W. P. Ding and D. Feng, *Large Magnetic entropy*, 1997.
- 43 P. G. Radaelli, D. E. Cox, M. Marezio, S.-W. Cheong, P. E. Schiffer and A. P. Ramirez, Simultaneous Structural, Magnetic, and Electronic Transitions in  $La_{1-x}Ca_xMnO_3$  with  $x = 0.25$  and  $0.50$ , *Phys. Rev. Lett.*, 1995, **75**, 4488–4491.
- 44 V. Franco, J. S. Blázquez and A. Conde, Field dependence of the magnetocaloric effect in materials with a second order phase transition: a master curve for the magnetic entropy change, *Appl. Phys. Lett.*, 2006, **89**, 222512.
- 45 Y. Xu, M. Meier, P. Das, M. R. Koblischka and U. Hartmann, Perovskite manganites: potential materials for magnetic cooling at or near room temperature, *Cryst. Eng.*, 2002, **5**, 383–389.
- 46 S. Ridha, D. Essebt and E. K. Hlil, Impact of Annealing Temperature on the Physical Properties of the Lanthanum Deficiency Manganites, *Crystals*, 2017, **7**, 301.
- 47 Ah. Dhahri, M. Jemmali, E. Dhahri and M. A. Valente, Structural characterization, magnetic, magnetocaloric properties and phenomenological model in manganite  $La_{0.75}Sr_{0.1}Ca_{0.15}MnO_3$  compound, *J. Alloys Compd.*, 2015, **638**, 221–227.
- 48 V. K. Pecharsky and K. A. Gschneidner, Some common misconceptions concerning magnetic refrigerant materials, *J. Appl. Phys.*, 2001, **90**, 4614–4622.
- 49 V. Franco, A. Conde, V. Provenzano and R. D. Shull, Scaling analysis of the magnetocaloric effect in  $Gd_5Si_2Ge_{1.9}X_{0.1}$  ( $X = Al, Cu, Ga, Mn, Fe, Co$ ), *J. Magn. Magn. Mater.*, 2010, **322**, 218–223.
- 50 V. Franco, A. Conde, J. M. Romero-Enrique and J. S. Blázquez, A universal curve for the magnetocaloric effect: an analysis based on scaling relations, *J. Phys.: Condens. Matter*, 2008, **20**, 285207.

